Biochemical and Biophysical Research Communications 461 (2015) 14–20

Contents lists available at ScienceDirect

Biochemical and Biophysical Research Communications

journal homepage: www.elsevier.com/locate/ybbrc

Crystal structures of YfiR from *Pseudomonas aeruginosa* in two redox states

Xuan Yang [a, 1], Xiu-an Yang [b, c, 1], Min Xu [b], Lei Zhou [b, c], Zusen Fan [a, **], Tao Jiang [b, *]

[a] Chinese Academy of Sciences Key Laboratory of Infection and Immunity, Institute of Biophysics, Chinese Academy of Sciences, Beijing 100101, PR China
[b] National Laboratory of Biomacromolecules, Institute of Biophysics, Chinese Academy of Sciences, Beijing 100101, PR China
[c] University of Chinese Academy of Sciences, Beijing 100049, PR China

ARTICLE INFO

Article history:
Received 11 March 2015
Available online 4 April 2015

Keywords:
Biofilm
YfiBNR
YfiR
c-di-GMP
Disulfide bond
Redox

ABSTRACT

YfiBNR is a recently identified c-di-GMP regulatory system involved in bacterial biofilm formation. The periplasmic protein YfiR inhibits the diguanylate cyclase activity of the inner membrane protein YfiN, whereas YfiB in the outer membrane can release this inhibition by sequestration of YfiR. In addition, this system may respond to anoxic conditions via YfiR, although the detailed mechanism is still unknown. Here we report crystal structures of *Pseudomonas aeruginosa* YfiR in the absence and presence of oxidative glutathione. Our structures reveal the overall folding of YfiR for the first time and demonstrate that YfiR exist as a dimer. Comparison of the two structures in different redox states revealed a broken/formation of one disulfide bond (Cys71-Cys110) and local conformational change around the other one (Cys145-Cys152). Mutagenesis studies indicated that Cys145-Cys152 plays an important role in maintaining the correct folding of YfiR.

1. Introduction

Biofilms are adherent communities of bacteria within a self-secreted extracellular matrix. Biofilms provide physical protection to pathogenic bacteria, facilitating evasion of the host immune system and rendering antibiotics ineffective [1–3]. The bacterial second messenger cyclic-di-GMP (c-di-GMP) is a positive regulator of the biofilm lifestyle of bacteria [4,5]. c-di-GMP is synthesized from GTP by diguanylate cyclases (DGCs), which contain a GG [D/E]EF active site, and hydrolyzed to pGpG by c-di-GMP-specific phosphodiesterases (PDEs), which contain either an EAL or HD-GYP domain [5–8]. In gram-negative bacteria such as *Pseudomonas aeruginosa, Escherichia coli*, *Klebsiella pneumoniae* and *Yersinia pestis*, a c-di-GMP signaling module called the YfiBNR system [9–15], also referred to as AwsXRO [16,17] or Tbp [18], has been identified and extensively characterized [9,11,12]. YfiN is located in the inner membrane and contains a periplasmic PAS domain and a cytosolic domain with presumable DGC activity [9,12]. YfiN is repressed by the specific interaction of its PAS domain with the periplasmic protein YfiR [9]. YfiB is an outer-membrane lipoprotein [16] that can activate YfiN by sequestering YfiR [9]. The c-di-GMP produced by YfiN increases the expression of the Pel and Psl exopolysaccharides, resulting in an small colony variant (SCV) phenotype characterized by surface attachment [9]. Previous compensatory mutagenesis studies have revealed that YfiR interacts directly with YfiN and that the residues involved in this interaction are located at the C-terminal region of YfiR [11]. Although the detailed mechanism remains elusive, the sequestration of YfiR and activation of YfiN may be induced by a YfiB-mediated cell wall stress-sensing mechanism [9,11,12]. In addition, a YfiB-independent regulation mechanism has been proposed in which YfiR activates YfiN in response to the redox status of the periplasm [11,19]. In gram-negative bacteria, DsbA is the primary bacterial machinery catalyzing the formation of disulfide bonds in the periplasm [20–23]. Deletion of DsbA produces a strong SCV phenotype in both Δ*yfiB* and wild type *P. aeruginosa* PAO1 but not a Δ*yfiBNR* strain [11], suggesting that correct disulfide bond formation plays a role in the YfiR-YfiN system independent of YfiB. Consistent with this observation, in *E. coli*, the absence of a disulfide bonding system (DBS) including DsbA and DsbB or the presence of DTT results in YfiR instability [19]. There are four conserved cysteine residues in YfiR and none

* Corresponding author. Fax: +86 10 64888510.
** Corresponding author. Fax: +86 10 64871293.
E-mail addresses: fanz@moon.ibp.ac.cn (Z. Fan), tjiang@ibp.ac.cn (T. Jiang).
[1] These authors contribute equally to this work.

http://dx.doi.org/10.1016/j.bbrc.2015.03.160
0006-291X/

in the predicted periplasmic portion of YfiN, and thus misfolding of YfiR caused by failed disulfide bond formation may induce the activation of YfiN.

With the exception of the C-terminal GGDEF domain of YfiN [12], no structural data are available for this system. In this study, we solved crystal structures of *P. aeruginosa* YfiR in its non-oxidized and oxidized states. The structure of the YfiR monomer is similar in the two structures, however, the four conserved cysteine residues, Cys71, Cys110, Cys145 and Cys152, are in different states. Cys71 and Cys110 form a disulfide bond in the oxidized form but maintain their free form in the non-oxidized YfiR structure. The Cys145-Cys152 disulfide bond is well formed in both structures, but the β5–β6 loop (141–149aa) where the Cys145 is located exhibits different conformations.

2. Materials and methods

2.1. Protein cloning, expression and purification

P. aeruginosa YfiR (residues 35–190, lacking the predicted N-terminal periplasm localization signal) was cloned into ORF1 of the pETDuet-1 (Merck Millipore, Darmstadt, Germany) vector via the BamHI and HindIII restriction sites with a constructed N-terminal His_6 and TEV cleavage site. Site-directed mutagenesis was performed using the QuikChange kit (Agilent Technologies, Santa Clara, CA) following the manufacturer's instructions.

Proteins were expressed in *E. coli* BL21-CodonPlus(DE3)-RIPL. Protein expression was induced by adding 0.5–1 mM IPTG at an OD600 of approximately 0.8. Cell cultures of wild type and mutated YfiR were incubated for an additional 4.5 h at 37 °C whereas Selenomethionine-substituted YfiR cell cultures were incubated at 16 °C for 18 h. The cells were then harvested by centrifugation and stored at −80 °C.

Cell suspensions were thawed and homogenized using a high-pressure homogenizer (JNBIO, People's Republic of China). The proteins were first purified by Ni affinity chromatography and then incubated with His6-tagged TEV protease overnight. The His_6-TEV protease and cleaved tag were subsequently removed by incubation with Ni-NTA resin. Finally, the proteins were purified using a Hi-TrapS^{TM} column (GE Healthcare) followed by a Superdex 200 (GE Healthcare) column. The purified fractions were collected and concentrated to 40 mg/ml in 20 mM Tris–HCl pH 8.0, 200 mM NaCl, frozen in liquid nitrogen and stored at −80 °C.

2.2. Crystallization and data collection

Crystal screening was performed by the sitting drop vapor diffusion method using commercial screening kits (Hampton Research, California, USA), and positive hits were optimized by the hanging drop vapor diffusion method at 293 K. Selenomethionine-substituted (SeMet) crystals of the YfiR protein were obtained and optimized in 0.1 M HEPES pH 7.5, 1.8 M ammonium sulfate. Oxidized YfiR crystals were obtained by soaking in 2 mM oxidative glutathione for 20 h. For cryoprotection, the crystals were soaked in 2.5 M lithium sulfate monohydrate for a few seconds and then flash-cooled in liquid nitrogen before data collection at a synchrotron-radiation source. The methods of crystal screen, optimization and the crystallization conditions of C110S were totally the same with that of wild type YfiR. Diffraction data for non-oxidized YfiR and the C110S mutant were collected on beamline BL17U at SSRF (Shanghai Synchrotron Radiation Facility), and data for oxidized YfiR were collected at a home-source Rigaku FR-E/VariMax X-ray generator. The diffraction data were processed using the HKL2000 software program [24].

2.3. Structure determination and refinement

The non-oxidized YfiR crystal belonged to space group $P4_32_12$ with a dimer in the asymmetric unit. The structure was solved by the Single-wavelength Anomalous Diffraction (SAD) method at 2.6 Å resolution using selenomethionine-substituted protein crystals [25]. The C110S mutant crystal belonged to space group $P4_32_12$ with a dimer in the asymmetric unit. The structure was solved by molecular replacement [26] at 2.45 Å resolution. The oxidized YfiR crystal belonged to space group $P4_32_12$ with two dimers in the asymmetric unit. The structure was solved by molecular replacement [26] at 3.2 Å resolution. Model building was performed using COOT [27] and refined with PHENIX [28]. The final structure was analyzed using PROCHECK [29]. The data collection and refinement statistics are presented in Table 1. Structure figures were prepared using PyMol (http://www.pymol.org) [30], and the coordinates have been deposited in the PDB under accession codes of 4YN7,4YN9 and 4YNA.

2.4. Analytical ultracentrifugation

Sedimentation velocity measurements were performed in a Beckman ProteomeLab XL-I at 25 °C. All protein samples were diluted to an OD 280 nm of 0.7 in 20 mM Tris, pH 8.0, 200 mM NaCl. Data were collected at 60,000 r.p.m. (262,000 g) every 3 min at a wavelength of 280 nm. Interference sedimentation coefficient distributions, c(M), were calculated from the sedimentation velocity data using SEDFIT [31].

3. Results and discussion

3.1. Overall structure of YfiR

The crystal structure of YfiR (residues 35 to 190; lacking the signal peptide) in the absence of oxidant was solved by Single-wavelength Anomalous Dispersion (SAD) method at 2.6 Å resolution using selenomethionine-substituted protein crystals. The crystal belongs to space group $P4_32_12$, with a dimer in the asymmetric unit. The final model includes residues 38–190 and is in good agreement with the diffraction data and expected geometric parameters (Table 1).

YfiR forms a globular compact structure composed of a seven-stranded β-sheet sandwiched by six peripheral α-helices (α1-6). The strand topology is 2-3-1-4-5-6-7 with strands 2 and 7 anti-parallel to the rest (Fig. 1A–B). Structural homology searches using the DALI server revealed that YfiR shares the highest structural similarity (Z-score of 11.6) with a substrate-binding subunit of a putative ABC transporter in *Streptococcus pneumonia* (PDB code 3LFT, unpublished). The ABC substrate-binding protein contains two domains, the N-terminal and C-terminal domains, which resemble each other and share structural similarities with the YfiR dimer (Fig. 1D–E). The r.m.s.d. value is 2.8 Å for 113 aligned Cα atoms between the C-terminal domain and YfiR monomer and 4.2 Å for 72 Cα atoms aligned between the N-terminal domain and YfiR monomer. However, the relative orientation of the two domains of the ABC protein is distinct from that of the two monomers in the YfiR dimer (Fig. 1D–E). Notably, the ABC protein binds L-Trp at the interface between the two domains (Fig. 1D–E), suggesting that YfiR binds small molecules that remain to be identified.

3.2. YfiR exists as a dimer in both the crystal and solution

In the crystal structure, two YfiR molecules form a stable dimer as shown in Fig. 1B. The dimerization interactions are composed of salt bridges formed by R98 and D80 from each monomer as well as

Table 1
Data-collection, phasing and refinement statistics.

Data collection	Non-oxidized YfiR	Oxidized YfiR	YfiR (C110S)
Space group	$P4_32_12$	$P4_32_12$	$P4_32_12$
Wavelength (Å)	0.97889	1.54187	0.97922
Resolution (Å)[a]	50.0–2.6 (2.64–2.6)	50.0–3.2 (3.26–3.2)	50.0–2.45 (2.49–2.45)
Cell dimensions			
a, b, c (Å)	120.72, 120.72, 87.46	119.67, 119.67, 85.78	121.01,121.01, 86.51
α, β, γ (°)	90, 90, 90	90, 90, 90	90, 90, 90
Unique reflections	20,544 (988)	10,704(510)	23,583 (1158)
I/σI	37.5 (10.64)	10.42 (3.26)	27.8 (4.6)
Completeness (%)	99.9 (100)	98.9 (100)	97.3 (98.0)
R_{merge} (%)	8.8 (49.7)	16.4 (48.6)	6.9 (38.1)
Wilson B factor (Å^2)	27.2	60.8	30.2
Refinement			
R_{work} (%)	18.94	24.63	18.85
R_{free}(%)	23.38	28.08	23.45
Average B factors (Å^2)			
Molecule A	28.87	45.45	32.58
Molecule B	35.56	58.39	41.60
Molecule C	–	144.12	–
Molecule D	–	136.38	–
$SO4^{2-}$	34.63	56.83	31.79
water	35.94	–	37.70
Root mean square deviations			
Bond lengths (Å)	0.013	0.010	0.008
Bond angles (°)	1.239	1.443	1.035
Ramachandran plot			
Most favored (%)	96.1	94.9	95.7
Additionally allowed (%)	3.9	5.1	4.3
Generously allowed (%)	0	0	0
Disallowed	0	0	0

Note: a, Numbers in parentheses are for the highest resolution shell.

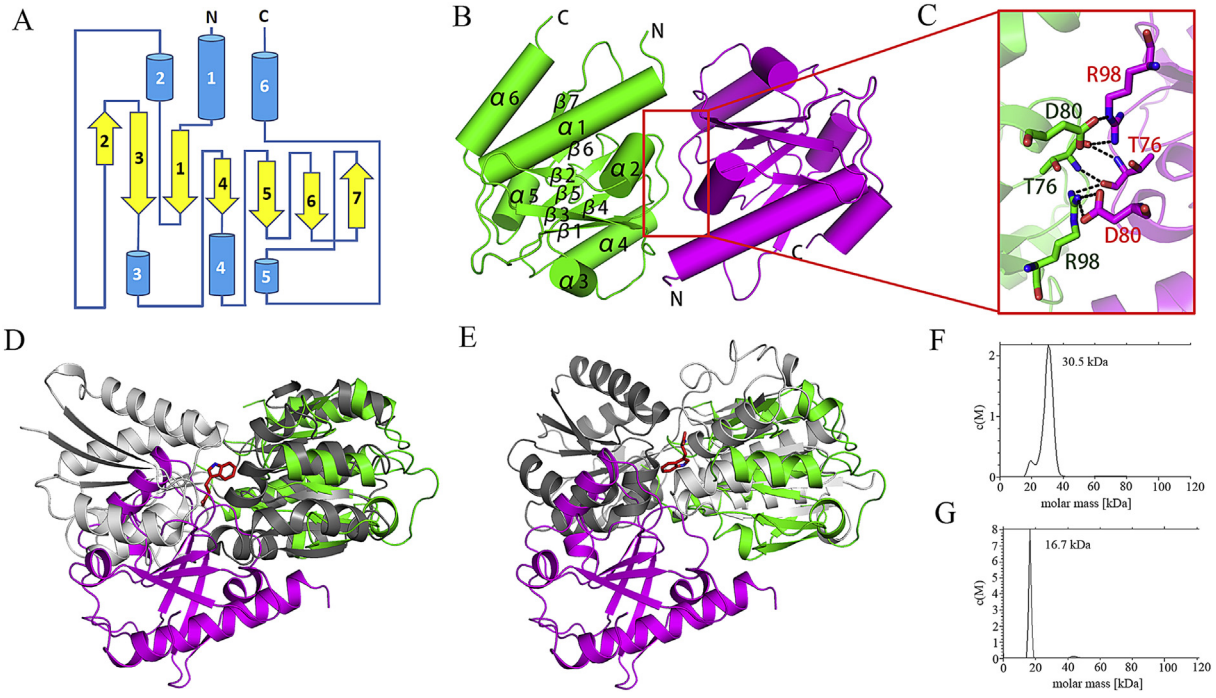

Fig. 1. Overall structure of YfiR, structural comparison of the YfiR dimer with the ABC substrate-binding protein, and dimerization of YfiR. (A) Topological diagram of the YfiR monomer. (B) Overall structure of the YfiR dimer per asymmetric unit. (C) Interaction residues at the interface of the YfiR dimer are labeled and shown in stick representation. (D–E) The N-terminal and C-terminal domains of the ABC substrate binding protein are each superposed on molecule A of the YfiR dimer. The bound L-Trp is shown in red stick form in a pocket formed between the two domains of the ABC substrate-binding protein. Molecules A and B of the YfiR dimer are shown in green and magenta, respectively. The N-terminal and C-terminal domains of the ABC substrate-binding protein are shown in light grey and deep grey, respectively. (F) Analytical ultracentrifugation of wild type YfiR. (G) Analytical ultracentrifugation of the R98A mutant of YfiR. (For interpretation of the references to color in this figure legend, the reader is referred to the web version of this article.)

hydrogen bond interactions between the main chains of T76 from each monomer (Fig. 1C). These interactions contribute to the majority of the dimer interface, with a buried surface area of 702.4 Å^2, suggesting that the dimeric state of YfiR is stable.

Consistently, analytical ultracentrifugation indicated that wild type YfiR had a calculated molecular mass of 30.5 kDa, close to the theoretical molecular weight of a YfiR dimer (34.7 kDa), indicating that YfiR exists as a dimer in solution (Fig. 1F). To validate the YfiR dimerization observed in the crystal structure and in solution, the dimerization residue mutant R98A was constructed. Analytical ultracentrifugation revealed that the R98A mutant had a calculated molecular mass of 16.7 kDa, close to the theoretical monomeric molecular weight of YfiR (17.4 kDa) (Fig. 1G). Our structural and biochemical data demonstrate that YfiR exists and likely functions in dimeric form as shown in the crystal structure.

3.3. Disulfide bonds in YfiR

The YfiBNR system may sense anoxic states through YfiR, hence promoting biofilm formation when oxygen is lacking [9,10]. To better understand the effect of redox status on YfiR, we analyzed the four cysteines in our YfiR structure. One pair (Cys145-Cys152) forms a disulfide bond, while the other (Cys71-Cys110) does not (Fig. 2). The distance between the two sulfate atoms in Cys71 and Cys110 is approximately 3.7 Å (Fig. 2C), which is longer than the standard disulfide bond length (usually 2.0–2.1 Å).

To elucidate the structural role of these two pairs of cysteines in YfiR folding, we introduced two single point mutations (C110S, C145A). The expression level of the C145A mutant was dramatically reduced. Taken together with the reduction in YfiR expression in the absence of DsbA [11], the reduced expression of the C145A mutant suggests that the absence of this disulfide bond may play an important role in YfiR misfolding. By contrast, the expression level of the C110S mutant was nearly identical to that of wild type YfiR, and C110S behaved similarly to wild type YfiR in a gel filtration experiment. To further ascertain whether the structure of the C110S mutant is similar to that of wild type YfiR, we crystallized the C110S mutant and solution of its structure by molecular replacement revealed that the structure of the C110S mutant is nearly identical to that of wild type (Fig. 3A and C).

Analysis of the structure around residues Cys71 and Cys110 revealed that the Cys71-containing β1 strand and the β4 strand following the Cys110-containing α3 helix are parallel to each other and form several main-chain hydrogen bonds. Therefore, the local structure remains stable even if the disulfide bond is broken (Fig. 2D). By contrast, the disulfide bond between Cys145 on the β5–β6 loop (141–149aa) and Cys152 on the β6 strand is the main force maintaining the local structure. Collectively, we propose that disruption of this disulfide bond will result in local disorder that may impair the stability or correct folding of YfiR, whereas the Cys71-Cys110 disulfide bond is not essential for correct folding.

3.4. The oxidized form of YfiR in the presence of oxidative glutathione

Because YfiR lacking a signal peptide was expressed in a relatively reductive cytoplasmic environment, we proposed that the Cys71-Cys110 disulfide bond may be formed in a normal periplasmic environment that is more oxidative. To verify the formation of the Cys71-Cys110 disulfide bond in an oxidative environment, we attempted to obtain the oxidized form of YfiR by soaking the native crystals (referred to as non-oxidized crystals for convenience) with

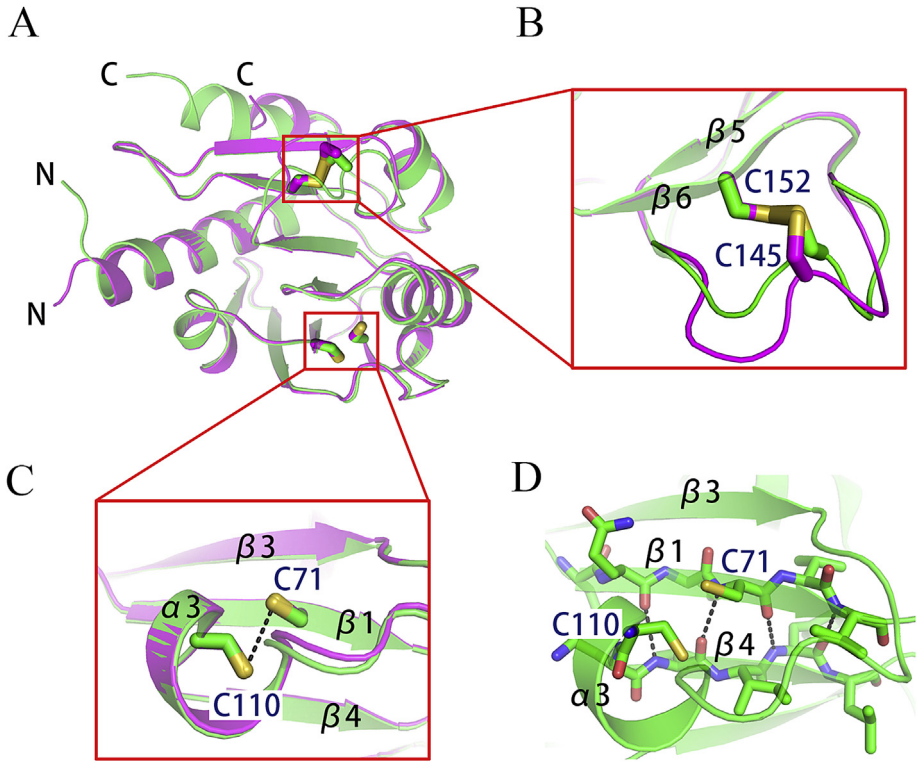

Fig. 2. The four cysteines in YfiR. (A) Structural superposition of two molecules in the YfiR dimer. The four cysteines found in the YfiR dimer are shown in stick form. (B) The intramolecular disulfide bonds formed between Cys145 and Cys152 are labeled and shown in stick form. The Cys145-containing β5–β6 loops are flexible. (C) The Cys71-Cys110 pair that does not form a disulfide bond is labeled and shown. (D) The hydrogen bonds formed between the Cys71-containing β1 strand and the β4 strand following the Cys110-containing α3 helix are shown as dark dotted lines. The electron density is contoured at 1.0σ in the 2|Fo|-|Fc| map.

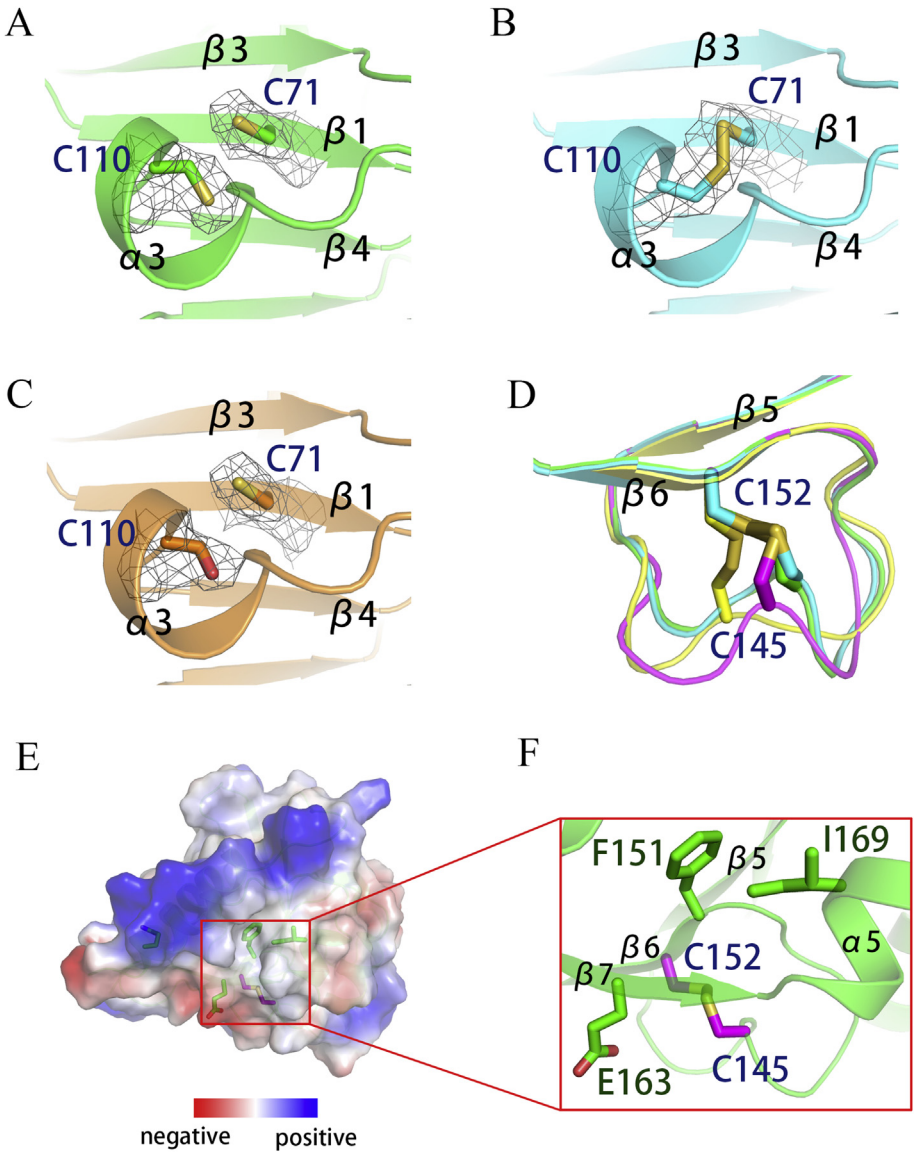

Fig. 3. Cysteine pairs in the non-oxidized form, oxidized form and C110S mutant of YfiR and proposed YfiN binding sites of YfiR. (A) The Cys71-Cys110 pair does not form a disulfide bond in non-oxidized YfiR. (B) The Cys71-Cys110 pair forms a disulfide bond in oxidized YfiR. (C) The Cys71-Cys110 pair does not form a disulfide bond in the C110S mutant of YfiR. (D) The Cys145-containing β5–β6 loops in non-oxidized and oxidized YfiR. Molecules A and B in the non-oxidized YfiR dimer are shown in green and magenta, respectively, whereas molecules A and B in the oxidized YfiR dimer are shown in cyan and yellow, respectively. (E) The net charge distribution on the surface of the YfiR monomer. The proposed YfiN binding sites of YfiR are shown as green sticks. The Cys145-Cys152 disulfide bond is shown as magenta sticks. (F) Close-up view of the locations of the proposed YfiN binding residues F151/E163/I169 and the nearby Cys145-Cys152 disulfide bond. (For interpretation of the references to color in this figure legend, the reader is referred to the web version of this article.)

oxidative glutathione. After soaking in 2 mM oxidative glutathione for 20 h, the oxidized crystals were used for data collection. Although the oxidized crystal belongs to space group $P4_32_12$ with nearly identical cell parameters as the non-oxidized crystal, an additional dimer can be observed in the asymmetric unit of oxidized YfiR (Fig. 4B). The second dimer of the oxidized YfiR structure has weaker electron density and a higher average B value, suggesting that it has certain flexibility within the crystalline lattice.

In contrast to the weak electron density of the second dimer, which prevented the construction of an unambiguous conformation of the two disulfide bonds, the electron density of the first dimer was pretty good. The Cys71-Cys110 pair indeed forms a disulfide bond as predicted (Fig. 3B), and the Cys145-Cys152 disulfide bond remains well preserved (Fig. 3D). Structural comparison revealed that the local conformation around Cys71-Cys110 is similar regardless of disulfide bond formation, further indicating the rigidity of this region. The absence of the second dimer in the non-oxidized structure remains an open question (Fig. 4A). One possible explanation is that YfiR may have greater structural flexibility in the non-oxidized state, resulting in multiple orientations or conformations in the crystal. Previous studies have indicated that the absence of the DBS disulfide bonding system or the presence of DTT destabilizes YfiR in *P. aeruginosa* and *E. coli* [11,20], and we propose that this disruption is mainly attributable to the disruption of Cys145-Cys152.

Curiously, although the Cys145-Cys152 disulfide bond is conserved, the β5–β6 loop around Cys145 is flexible and adopts different conformations in the above-mentioned structures (Fig. 3D). Malone JG et al. have reported that F151, E163, I169 and

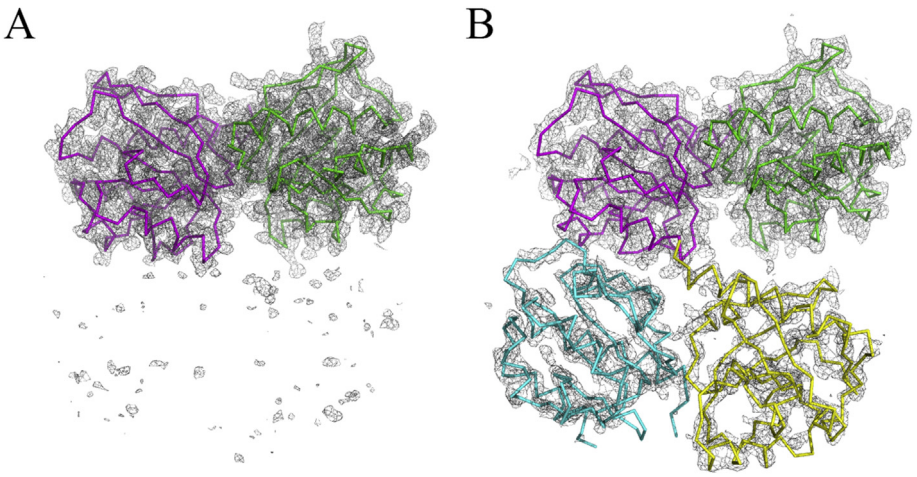

Fig. 4. Electron density comparison of non-oxidized and oxidized forms of YfiR. (A) The electron density of non-oxidized YfiR. (B) The electron density of oxidized YfiR. Molecules A and B of the first dimer are shown in green and magenta, respectively. Molecules C and D of the second dimer are shown in cyan and yellow, respectively. (For interpretation of the references to color in this figure legend, the reader is referred to the web version of this article.)

Q187 near the C-terminus of YfiR represent a putative YfiN binding site [11]. Plotting these residues onto the YfiR structure revealed that residues F151, E163 and I169 form a hydrophobic pocket, while Q187 is located at the end of the α6 helix, which is more distant (Fig. 3E–F). Interestingly, structural analysis revealed that residues F151, E163 and I169 are close to the Cys145-Cys152 disulfide bond (Fig. 3F). In particular, F151 and Cys152 are both on the β6 strand, which is antiparallel to the E163-containing β7 strand. The structural flexibility around Cys145-ys152 may facilitate/affect the interaction of YfiR with YfiN such that under extremely reductive conditions, the loss of the Cys145-Cys152 disulfide bond may result in impaired YfiN-binding ability or degradation of misfolded YfiR, triggers the activation of YfiN.

Collectively, we present the YfiR structure in both the non-oxidized and oxidized states, unraveling that the Cys145-Cys152 disulfide bond plays an essential role in maintaining the correct folding of YfiR and is close to the putative YfiN binding site. Moreover, structural comparison revealed that the YfiR dimer shares similarity with the substrate binding subunit of an ABC transporter which can recognize L-Trp. These observations provide a structural basis and new clues for future investigations of how YfiR-related allosteric regulation occurs in response to redox variation and small-molecule signals.

Disclosures

All authors declare no financial competing interests.
All authors declare no non-financial competing interests.

Conflict of interest

None.

Acknowledgments

We acknowledge the staff at the BL17U beamline of the SSRF (Shanghai Synchrotron Radiation Facility) in China for technical assistance during data collection. We thank Xiaoxia Yu for her support in the experiment of analytical ultracentrifugation. This work was supported by grants from and the National Natural Science Foundation of China; The Strategic Priority Research Program (XDB08010301).

Transparency document

Transparency document related to this article can be found online at http://dx.doi.org/10.1016/j.bbrc.2015.03.160.

References

[1] J.W. Costerton, Introduction to biofilm, Int. J. Antimicrob. Agents 11 (1999) 217–221 [discussion 237–219].
[2] J.W. Costerton, P.S. Stewart, E.P. Greenberg, Bacterial biofilms: a common cause of persistent infections, Science 284 (1999) 1318–1322.
[3] P.D. Newell, C.D. Boyd, H. Sondermann, G.A. O'Toole, A c-di-GMP effector system controls cell adhesion by inside-out signaling and surface protein cleavage, PLoS Biol. 9 (2011) e1000587.
[4] P. Ross, H. Weinhouse, Y. Aloni, D. Michaeli, P. Weinberger-Ohana, R. Mayer, S. Braun, E. de Vroom, G.A. van der Marel, J.H. van Boom, M. Benziman, Regulation of cellulose synthesis in acetobacter xylinum by cyclic diguanylic acid, Nature 325 (1987) 279–281.
[5] P. Ross, R. Mayer, M. Benziman, Cellulose biosynthesis and function in bacteria, Microbiol. Rev. 55 (1991) 35–58.
[6] R.P. Ryan, Y. Fouhy, J.F. Lucey, L.C. Crossman, S. Spiro, Y.W. He, L.H. Zhang, S. Heeb, M. Camara, P. Williams, J.M. Dow, Cell-cell signaling in Xanthomonas campestris involves an HD-GYP domain protein that functions in cyclic di-GMP turnover, Proc. Natl. Acad. Sci. U S A 103 (2006) 6712–6717.
[7] Z.T. Guvener, C.S. Harwood, Subcellular location characteristics of the Pseudomonas aeruginosa GGDEF protein, WspR, indicate that it produces cyclic-di-GMP in response to growth on surfaces, Mol. Microbiol. 66 (2007) 1459–1473.
[8] T. Schirmer, U. Jenal, Structural and mechanistic determinants of c-di-GMP signalling, Nat. Rev. Microbiol. 7 (2009) 724–735.
[9] J.G. Malone, T. Jaeger, C. Spangler, D. Ritz, A. Spang, C. Arrieumerlou, V. Kaever, R. Landmann, U. Jenal, YfiBNR mediates cyclic di-GMP dependent small colony variant formation and persistence in Pseudomonas aeruginosa, PLoS Pathog. 6 (2010) e1000804.
[10] V. Sanchez-Torres, H. Hu, T.K. Wood, GGDEF proteins Yeal, YedQ, and YfiN reduce early biofilm formation and swimming motility in Escherichia coli, Appl. Microbiol. Biotechnol. 90 (2011) 651–658.
[11] J.G. Malone, T. Jaeger, P. Manfredi, A. Dotsch, A. Blanka, R. Bos, G.R. Cornelis, S. Haussler, U. Jenal, The YfiBNR signal transduction mechanism reveals novel targets for the evolution of persistent Pseudomonas aeruginosa in cystic fibrosis airways, PLoS Pathog. 8 (2012) e1002760.
[12] R. Dobson, G. Giardina, A. Paiardini, S. Fernicola, S. Franceschini, S. Rinaldo, V. Stelitano, F. Cutruzzolà, Investigating the allosteric regulation of YfiN from Pseudomonas aeruginosa: clues from the structure of the Catalytic domain, PLoS One 8 (2013) e81324.
[13] E.L. Raterman, D.D. Shapiro, D.J. Stevens, K.J. Schwartz, R.A. Welch, Genetic analysis of the role of yfiR in the ability of Escherichia coli CFT073 to control cellular cyclic dimeric GMP levels and to persist in the urinary tract, Infect. Immun. 81 (2013) 3089–3098.
[14] M.G. Huertas, L. Zarate, I.C. Acosta, L. Posada, D.P. Cruz, M. Lozano, M.M. Zambrano, Klebsiella pneumoniae yfiRNB operon affects biofilm formation, polysaccharide production and drug susceptibility, Microbiology 160 (2014) 2595–2606.

[15] G.X. Ren, H.Q. Yan, H. Zhu, X.P. Guo, Y.C. Sun, HmsC, a periplasmic protein, controls biofilm formation via repression of HmsD, a diguanylate cyclase in Yersinia pestis, Environ. Microbiol. 16 (2014) 1202–1216.
[16] S.R. Giddens, R.W. Jackson, C.D. Moon, M.A. Jacobs, X.X. Zhang, S.M. Gehrig, P.B. Rainey, Mutational activation of niche-specific genes provides insight into regulatory networks and bacterial function in a complex environment, Proc. Natl. Acad. Sci. U S A 104 (2007) 18247–18252.
[17] H.J. Beaumont, J. Gallie, C. Kost, G.C. Ferguson, P.B. Rainey, Experimental evolution of bet hedging, Nature 462 (2009) 90–93.
[18] A. Ueda, T.K. Wood, Connecting quorum sensing, c-di-GMP, pel polysaccharide, and biofilm formation in Pseudomonas aeruginosa through tyrosine phosphatase TpbA (PA3885), PLoS Pathog. 5 (2009) e1000483.
[19] D.A. Hufnagel, W.H. DePas, M.R. Chapman, The disulfide bonding system Suppresses CsgD-independent cellulose production in *Escherichia coli*, J. Bacteriol. 196 (2014) 3690–3699.
[20] A. Holmgren, M. Fagerstedt, The in vivo distribution of oxidized and reduced thioredoxin in *Escherichia coli*, J. Biol. Chem. 257 (1982) 6926–6930.
[21] J.C. Bardwell, K. McGovern, J. Beckwith, Identification of a protein required for disulfide bond formation in vivo, Cell 67 (1991) 581–589.
[22] J. Messens, J.F. Collet, Pathways of disulfide bond formation in Escherichia coli, Int. J. Biochem. Cell. Biol. 38 (2006) 1050–1062.
[23] M. Depuydt, J. Messens, J.F. Collet, How proteins form disulfide bonds, Antioxid. Redox Signal 15 (2011) 49–66.
[24] Z. Otwinowski, W. Minor, Processing of X-ray diffraction data collected in oscillation mode, Methods Enzymol. 276 (1997) 307–326.
[25] Z. Dauter, M. Dauter, E. Dodson, Jolly SAD, Acta Crystallogr. Sect. D. Biol. Crystallogr. 58 (2002) 494–506.
[26] A.A. Lebedev, A.A. Vagin, G.N. Murshudov, Model preparation in MOLREP and examples of model improvement using X-ray data, Acta. Crystallographica. Sec. D Biol. Crystallogr. 64 (2008) 33–39.
[27] P. Emsley, B. Lohkamp, W.G. Scott, K. Cowtan, Features and development of Coot, Acta Crystallogr. D. Biol. Crystallogr. 66 (2010) 486–501.
[28] P.D. Adams, P.V. Afonine, G. Bunkoczi, V.B. Chen, I.W. Davis, N. Echols, J.J. Headd, L.W. Hung, G.J. Kapral, R.W. Grosse-Kunstleve, A.J. McCoy, N.W. Moriarty, R. Oeffner, R.J. Read, D.C. Richardson, J.S. Richardson, T.C. Terwilliger, P.H. Zwart, PHENIX: a comprehensive Python-based system for macromolecular structure solution, Acta Crystallogr. D. Biol. Crystallogr. 66 (2010) 213–221.
[29] R.A. Laskowski, M.W. MacArthur, D.S. Moss, J.M. Thornton, PROCHECK: a program to check the stereochemical quality of protein structures, J. Appl. Crystallogr. 26 (1993) 283–291.
[30] W.L. Delano, The PyMOL Molecular Graphics System, DeLano Scientific, San Carlos, CA, USA, 2002.
[31] P. Schuck, Size-distribution analysis of macromolecules by sedimentation velocity ultracentrifugation and lamm equation modeling, Biophys. J. 78 (2000) 1606–1619.